Discover Chemical Engineering

Discover

Perspective

Chemical looping approaches to decarbonization via CO_2 repurposing

Collin Schmidt[1] · Hanzhong Shi[1] · Debtanu Maiti[2] · Bryan J. Hare[3] · Venkat R. Bhethanabotla[1] · John N. Kuhn[1]

Received: 23 May 2023 / Accepted: 4 July 2023
Published online: 01 August 2023

Abstract
Active areas of research on chemical looping technologies for the conversion of CO_2 to CO are contrasted and discussed**,** including current performance, methods for material design, and next steps in expanding their development. Generation of CO from CO_2 is of interest in sustainable chemistry and engineering to convert anthropogenic CO_2 emissions into feedstock for Fischer–Tropsch (FT), methanol to gasoline (MTG), gas-to-liquid (GTL), and other synthesis pathways for fuels and materials. Chemical looping strategies have been identified which not only produce CO, but also H_2 from H_2O and methane sources, supplying the other key component of syngas. Configurations of these chemical looping technologies into the materials economy potentially constitute sustainable carbon loop cycles for fuels as well as carbon sequestration into industrial and commercial materials. Major areas of research in CO_2 conversion by chemical looping, collectively referred to here as CO2CL, including Solar-Thermal Chemical Looping (STCL), Reverse Water Gas Shift Chemical Looping (RWGS-CL), Chemical Looping Reforming (CLR), Super Dry Reforming (SDR), Autothermal Catalyst Assisted Chemical Looping (ACACL), and Reverse Boudouard Reforming (RBR) are discussed in terms of their process characteristics, historical development of oxygen carrier (OC) material, state of the art methods for material design, and future work needed to advance the scale-up of these technologies. This perspective centers around the non-methane utilizing processes for CO2CL, focusing on the phenomena of oxygen transfer between gas molecules and the oxygen carrier (OC).

1 Introduction

An approach to mitigating the anthropogenic influence on climate change due to CO_2 accumulation in the atmosphere is the chemical conversion of CO_2. The United States government is working towards developing U.S. Long Term Strategy (LTS) for 100% carbon pollution free electricity by 2035 and net-zero GHG emissions. The recent decarbonization efforts are targeted towards all possible means of lowering industrial carbon footprints, which include developing chemical processes for repurposing waste CO_2 and CH_4. These two greenhouse gases are thermodynamically stable and dilute in the atmosphere. Chemical looping (CL) strategies for CO_2 repurposing (CO2CL) address the thermodynamic challenges by involving metal oxides in an oxygen transfer cycle to convert CO_2 to CO, wherein the metal oxide Gibbs energy of formation is even lower than that of CO_2, allowing for higher equilibrium conversion in a given stage of the chemical looping process, in this work referred to as the reduction or oxidation of the oxygen carrier (OC).

Separating the redox steps not only enables more control of each step, leading to higher yields and energy efficiency, but also eliminates the chance of secondary reactions between the primary products and reactants. Due to the closed thermodynamic cycle of the OC, the net reaction over the complete chemical looping cycle does not include the OC

✉ Venkat R. Bhethanabotla, bhethana@usf.edu; ✉ John N. Kuhn, jnkuhn@usf.edu | [1]Department of Chemical, Biological, and Materials Engineering, University of South Florida, Tampa, FL 33620, USA. [2]Catalysis and Transient Kinetics Group, Idaho National Laboratory, Idaho Falls, ID 83415, USA. [3]School of Chemical and Biomolecular Engineering, Georgia Institute of Technology, Atlanta, GA 30332, USA.

changing through oxygen deficiency, and as a result the overall equilibrium conversion is unchanged. However, process advantages can still be realized by leveraging the fact that species involved in the OC reduction and oxidation remain separated. This allows for significant reduction of complexities associated with separation of desired products, and recycling of product streams.

Conversion of CO_2 and CH_4 to CO and H_2 (key components of syngas) via CL approaches paves the way for high-value hydrocarbon generation via Fischer–Tropsch routes, making it a candidate for mitigating the effects of global warming and facilitating progress of the US LTS. Direct synthesis of methanol and plastics using CO as feedstock has also been demonstrated. The industrial decarbonization via CO2CL in the greater economy are illustrated in Fig. 1. Innovations and further progress lie in developing candidate materials for CL pathways for CO_2 reduction, probing fundamental mechanistic insights, and scale up efforts to improve predictions of performance at commercial scale.

2 CL pathways

The concept of CL revolves around decoupling the reduction and oxidation reactions on an oxygen-rich platform (the OC). Conceptually, the CL approaches split a single reactor process into multiple steps, by introducing a material which captures an intermediate species, allowing the same net reaction to be achieved in processes separated in space (separate reactors) or time (cycling gas feeds to a single reactor). In the case of CO2CL, the OC materials are intervening in the oxygen transfer from CO_2. The net reactions for the reduction gas and CO_2 remain the same, while the OC material cycles between oxidized or near stoichiometric state (MO_x) and oxygen-deficient reduced states ($MO_{x-\delta}$), written generally as the following equations.

$$\text{General reduction reaction}: \delta R_{(g)} + MO_x \rightarrow MO_{x-\delta} + \delta L \tag{1}$$

$$\text{General oxidation reaction}: \delta CO_2 + MO_{x-\delta} \rightarrow MO_x + \delta CO \tag{2}$$

In all cases of CO2CL discussed here, oxygen removed from the OC during the reduction step produces an oxygen containing gas molecule (L), which forms part of the reactor gas effluent. The RWGS-CL and methane utilizing CO2CL processes differ from STCL in that they utilize a reducing gas (R), which is involved in the chemistry of the material reduction, and provides some of the atoms in the leaving group molecule (L). The reducing gas (or lack thereof) and leaving group chosen for the oxygen introduce fundamental thermodynamic limitations to the process of OC reduction.

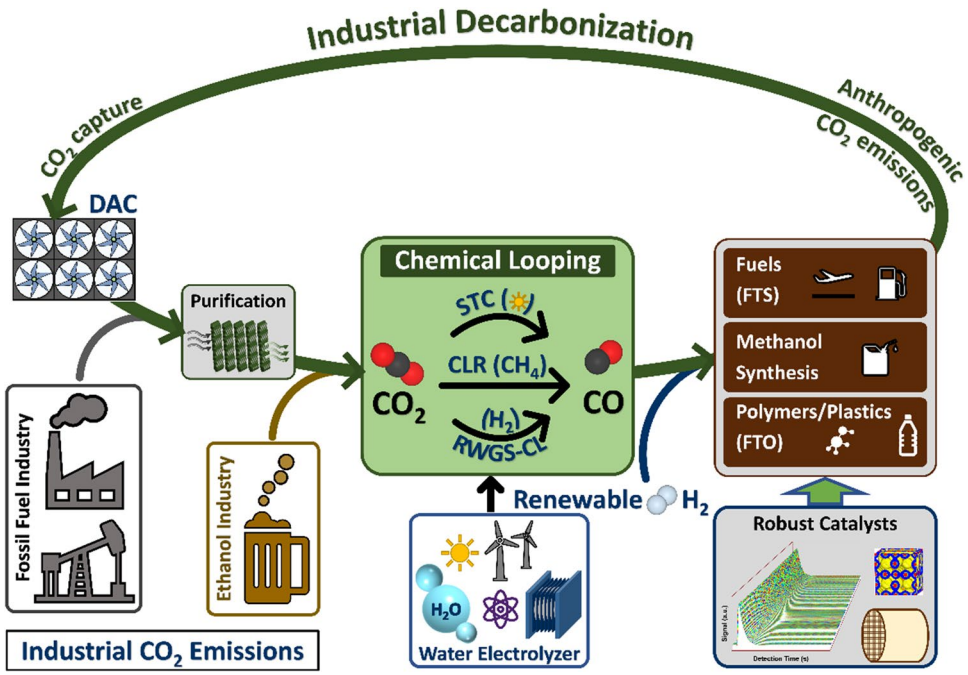

Fig. 1 Material pathways for Chemical Looping CO_2 to CO Conversion (CO_2CL) in the greater economy

RWGS-CL and methane utilizing CO2CL processes make use of hydrogen and methane, respectively, for the reducing gas, but both processes result in the net formation of water as the leaving group for oxygen from the OC. STCL does not utilize a reducing gas, and emits diatomic oxygen from the OC during reduction, excised from the OC lattice at very high temperatures under primarily-entropic driving forces. The inclusion of a reducing gas with net water production in the case of RWGS-CL and CLR incorporates the Gibbs formation energy of the water molecule, helping to drive equilibrium conversion forward in the reduction step, and allowing these processes to achieve OC reduction at lower temperature, as seen in Fig. 2. In all cases, the oxygen leaving the ionic solid in a gas phase molecule greatly increases the entropy of the products through the confined vibrational states available to an oxygen anion within the solid being converted to translational degrees of freedom exploring the gas phase volume.

Conversion of CO_2 to CO occurs over the reduced OC, wherein the solid material scavenges a single oxygen atom from each CO_2 molecule. As the reduction and oxidation steps are separated, a critical parameter for the performance of CO2CL is the extent of oxygen deficiency (δ) achieved during the reduction step, which ultimately determines the molar conversion of CO_2 to CO achievable for a single CL cycle. Common convention is for δ reaching 1 as each formula unit of OC is deficient a single oxygen atom. In practice, OC materials (e.g., simple metal oxides and complex ones such as perovskites and spinels, etc.) undergo permanent changes to their structure and chemical identity prior to δ reaching 1. Such a high extent of oxygen deficiency is not explored the thermodynamic cycle of CO2CL, where the severity of reduction conditions are chosen such that oxygen is removed without introducing permanent changes to the OC. The extent of reduction not only determines the amount of CO_2 that may be converted in a given CL cycle, but also dictates the concentration of sites and phases capable of removing oxygen from CO_2, thereby affecting the kinetics of reaction processes. While the maximum extent of reduction is an intrinsic thermodynamic characteristic of the material at a certain reaction condition, the time span of reaction and associated kinetic information governs the formation of reaction-relevant reduced phase ($MO_{x-\delta}$). The ability of these materials to circle back to a similar oxidized phase (MO_x) allows for sustainable operation of these CL cycles. These net reduction steps are shown below in Eqs. 3–6.

$$\mathrm{STCL}: \ \mathrm{MO_x} \rightarrow \mathrm{MO_{x-\delta}} + \delta\mathrm{O_2}(\text{high temperature}) \tag{3}$$

$$\mathrm{RWGS-CL}: \ \mathrm{MO_x} + \delta\mathrm{H_2} \rightarrow \mathrm{MO_{x-\delta}} + \delta\mathrm{H_2O} \tag{4}$$

$$\mathrm{CLR}: \ \mathrm{MO_x} + \mathrm{CH_4} \rightarrow \mathrm{MO_{x-\delta}} + \delta\mathrm{O\ removal}\left(\text{as CO, } \mathrm{CO_2}\text{, and } \mathrm{H_2O}\right) \tag{5}$$

The current status of the 3 CL approaches to CO_2 reduction is illustrated in Fig. 2. From both CO yield/gram of solid material and temperature of operation, RWGS-CL merits intense development for industrial implementation.

2.1 STCL

The STCL cycles generally operate in two separate steps, reduction and oxidation, utilizing a metal oxide material (MO) as a reactive intermediate. Here, the metal oxidate will be referred to as the oxygen carrier (OC), with common role across the discussed processes for CO2CL. The complete chemical looping cycle for STCL is shown in Table 1 with a particular formulation of perovskite oxide, which have been demonstrated to lower the reduction temperatures significantly [1]. The changes to a perovskite oxide OC are shown schematically in Fig. 3. Rather than the OC changing to a different

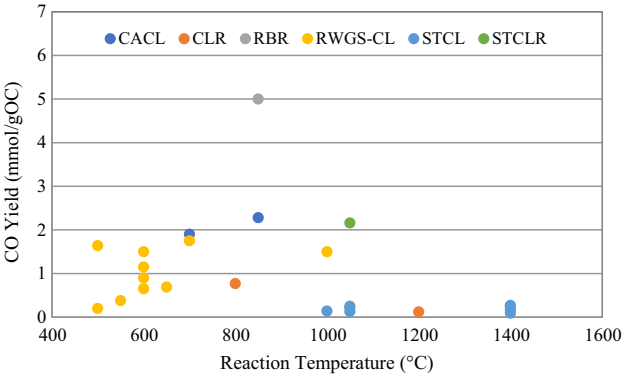

Fig. 2 Current state of the art on CO yield and operating temperature for the CO_2CL approaches, reflecting the data and citations listed in Sect. 3

Table 1 Summarized process for Solar Thermal Chemical Looping (STCL), utilizing perovskite as OC, reduced under high temperature, and forming syngas from mixed CO_2, H_2O feed

Solar Thermal Chemical Looping	Solid Loading and Gas Feed *(CL Stage)*	Major Reactions	Majority Effluent
	$La_{0.5}Sr_{0.5}MnO_3$ *(Initial Solids Loading)*	Gas / Solid: ABO_3 (Perovskite General Formula)	
	Inert *(Reduction Cycle)*	$ABO_3 \rightarrow ABO_{3-\delta} + \delta/2\ O_2$	Inert, O_2
	$CO_2 + H_2O$ *(Oxidation Cycle)*	$ABO_{3-\delta} + CO_2 \rightarrow ABO_3 + CO$; $ABO_{3-\delta} + H_2O \rightarrow ABO_3 + H_2$	CO, H_2, CO_2, H_2O

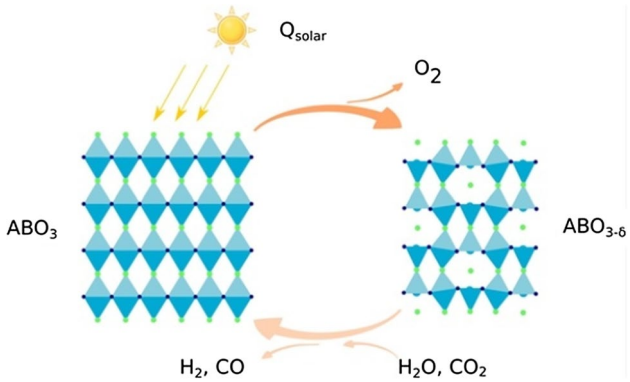

Fig. 3 Process schematic for STCL using a perovskite oxide (ABO_3) as the oxygen carrier (OC). Distortions of the perovskite lattice due to oxygen vacancies are schematically shown in the reduced state. However, new crystal geometries and even local phase changes may occur in CL processes (particularly at the high temperatures of STCL) in order to lower the energy of the oxygen deficient material. (Reproduced through MDPI Open Access [1])

crystal structure or metal oxide species, only local changes occur in the perovskite oxide upon low to moderate oxygen deficiency. Substitutional defects occur in the formation of vacancies at sites normally occupied by oxygen anions in the perfect crystal.

A variant of STCL utilizing methane reforming (here referred to as STCLR) at high temperature over ceria has also been investigated by Chuayboon [2]. The use of a CH_4 to generate H_2 as a reducing gas increases the oxygen transfer per chemical looping cycling.

Although STCL processes using binary oxides seem impractical given the high energy costs, more advanced alternative materials have demonstrated high activity at much lower temperatures. One series of optimized substituted iron-based spinels is $Fe_{3-x}A_xO_4$ (A = Mn, Co, Ni, Zn). The reduction behavior in this ferrite redox system can be manipulated by partial cation substitution of Fe in the spinel. The spinel substituted iron oxide can reduce the reaction temperature by > 100 °C (650–1100 °C). Similarly, spinel substituted perovskite oxide materials could also reduce the energy requirement for the reduction.

In addition to CO_2 to CO conversion, oxygen deficient perovskites and other OC materials are also capable of scavenging oxygen from water, leading to production H_2 (Fig. 3). Consequently, if sufficient renewable energy is available, CO2CL processes are capable of generating both the CO and H_2 components of syngas for material and fuel feedstocks.. While a single OC material choice and single reactor would reduce separation cost, separately designed materials and separately sized reactors for the H_2 and CO production would conceptually be able to produce specific ratios of H_2/CO syngas for downstream synthesis processes.

2.2 RWGS-CL

Rather than temperature alone to produce oxygen deficiency in the OC (as in the case of STCL), RWGS-CL uses H_2 as a reactant in the reduction step, producing H_2O (Fig. 4, Table 2) rather than O_2 as the net gas output (Fig. 3). During the reduction step, H_2 adsorbs and reacts with the solid to form H_2O, which desorbs, leaving point defects in the OC in the form of oxygen vacancies in the crystal lattice. During the oxidation step, CO_2 adsorbs on the OC and reacts with the oxygen vacancies, with an oxygen atom filling the lattice vacancy, and leaving CO to desorb as the gas product.

The common candidate materials for RWGS-CL are highly stable metal oxides, such as perovskite oxides. Perovskites have a general formula of ABO_3, wherein A and B are metal cation, with transition metals common for the B-site. Not all perovskites exhibit oxygen vacancy formation at low to moderate reduction conditions under H_2, such as $LaFeO_3$ [4]. As a result, partial substitutional defects of the A and B site are common in practice. Swapping out some of the A or B site metals with a different atom introduces strain to the material, as well as introducing electron acceptors and donors, and is the source of the 'tunable' nature of perovskite materials. Many perovskite formulations are capable of maintaining their crystal structure under oxygen deficiencies up to $\delta = 0.5$, making them attractive materials for the OC cycling without loss of surface area, or irreversible phase transitions over many cycles.

2.3 Methane utilizing CO2CL processes

A number of CO2CL processes have been developed which make use of methane abundant from petroleum of biological pathways to accomplish the reduction of the OC, typically by involving catalytic reactions with methane to produce hydrogen, which then directly reduces the OC. While the OC can be considered catalyst over the complete chemical looping cycle (i.e. returns to its starting thermodynamic state over the process), the OC acts as a solid reagent over the reduction or oxidation stages of the chemical looping process (i.e. undergoes stoichiometric alteration following extent of reaction). In contrast, methane utilizing CO2CL processes (such as SDR, ACACL, and RBR) typically use a complete catalytic process within one of the CL stages, without the OC intervening to separate the reaction into two stages.

2.3.1 Chemical looping reforming (CLR)

Chemical Looping Reforming (CLR) processes introducing an OC to typical reforming reactions between CO_2 and CH_4 have also been developed. Both air and CO_2 have been demonstrated as the oxidizing gas. The reducing gas in CLR is CH_4, which receives oxygen from the OC to produce CO, commonly referred to as Partial Oxidation of Methane (POM). The hydrogen content in the CH_4 also receives oxygen from the OC, producing water. The hydrogen content therefore interferes with the atom economy of CO production by competing for the same 'reagent' in the form of oxygen deficiency in the OC. However, involving the production of water incorporates its Gibbs formation energy and subsequently tilts the equilibrium forward.

Some versions of CLR utilize multiple chemical looping steps (Fig. 5), differing from STCL and RWGS-CL in that three steps are required to achieve the net reaction. The introduction of a carbon carrier (CC) in addition to the oxygen carrier (OC) captures CO_2 from a concentrated flue gas stream. An addition of methane is also used as the

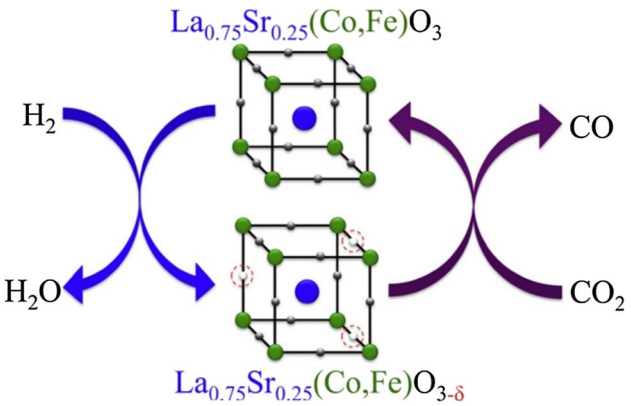

Fig. 4 Process schematic for RWGS-CL with a specific formulation of perovskite oxide as the oxygen carrier, which facilitates the transfer of oxygen from CO_2 to H_2O. As is typical in RWGS-CL, formation of limited oxygen vacancies in the perovskite may locally distort the crystal structure, but the cubic motif is maintained. (Reproduced with permission from Elsevier [3])

Table 2 Summarized process for Reverse Water Gas Shift Chemical Looping (RWGS-CL), utilizing perovskite as OC, and undergoing reduction from H_2 for direct production of syngas with CO_2, H_2O feed

Reverse Water Gas Shift Chemical Looping	Solid Loading and Gas Feed *(CL Stage)*	Major Reactions	Majority Effluent
	$La_{0.5}Sr_{0.5}FeO_3$ *(Initial Solids Loading)*	Gas / Solid: ABO_3 (Perovskite General Formula)	
	H_2 *(Reduction Cycle)*	δH_2 → δH_2O; ABO_3 → $ABO_{3-\delta}$	H_2O
	$CO_2 + H_2O$ *(Oxidation Cycle)*	CO_2 → CO; $ABO_{3-\delta}$ → ABO_3; H_2O → H_2; $ABO_{3-\delta}$ → ABO_3	CO, H_2, CO_2, H_2O

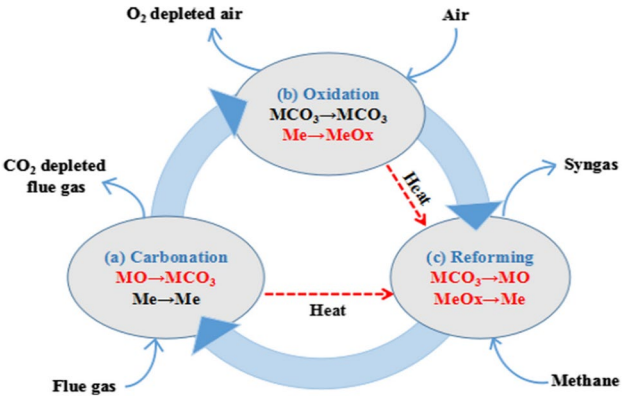

Fig. 5 Process schematic for CLR using both an oxygen carrier (OC) and carbon carrier (CC), in which the metal oxide is used to carry both oxygen and activated carbon species between chemical looping steps. CLR can also be accomplished using just an OC to interface in the oxygen transfer between CO_2 and CH_4. (Reproduced with permission from Elsevier [5])

reducing gas, allowing for the formation of H_2 and H_2O in the reforming step to produce syngas. Whether using an OC only or an OC and CC in tandem, CLR maintains the advantages of using a reduction gas in that the temperatures required are lower than STCL. However, the lower reduction severity of CH_4 as compared to H_2 puts CLR processes in general at intermediate temperatures between RWGS-CL and STCL.

While the additional chemical looping steps in the CLR process increases the complexity of material design, it also offers more opportunity for specializing the solid reactivity further.

2.3.2 Super dry reforming (SDR)

Super Dry Reforming makes use of a methane dry reforming catalyst bed in addition to OC and CO_2 sorbent in an adjacent bed. The configuration and materials investigated by Buelens [6] are summarized in Table 3. The dry reforming process occurs independently to the OC and sorbent reactions, with the mixed feed of CO_2 and CH_4 encountering the dry reforming bed prior to the products flowing over the CL/sorbent bed. Reduction of the metal oxide and capture of CO_2 are accomplished during the reduction stage, with H_2O as the primary effluent. In the oxidation step, an inert is flowed through the beds, which results in desorption of CO_2 for reaction with the reduced metal oxide OC to produce CO. A major advantage of the SDR process is the separate production of H_2O and CO, simplifying downstream product separation.

2.3.3 Catalyst assisted chemical looping (CACL)

Catalyst Assisted Chemical Looping (CACL) makes use of dry reforming catalyst and metal oxide OC in a mixed bed. The so-called "catalyst assistance" comes in the form of a dry reforming catalyst which converts CH_4 to H_2 for use as a reducing

Table 3 Summarized process for Super Dry Reforming (SDR) which utilizes a dry reforming catalyst in tandem with metal oxide as oxygen carrier (OC), and CaO as a CO_2 sorbent

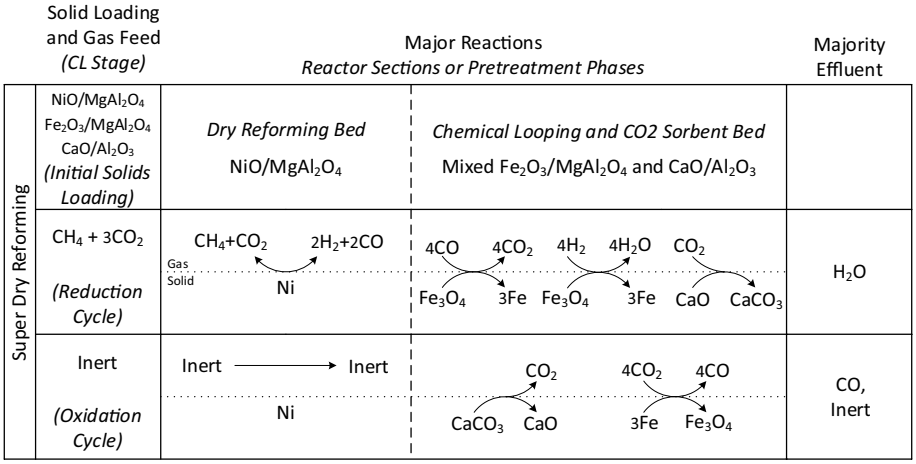

Table 4 Summarized process for Autothermal Catalyst Assisted Chemical Looping (ACACL), which utilizes dry reforming reactions and combustion of methane to produce syngas and satisfy heat demand, respectively

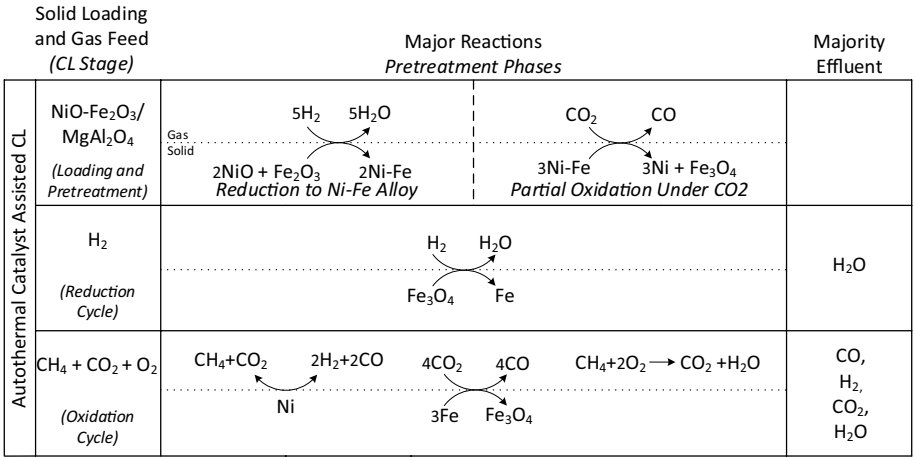

Table 5 Summarized process for Reverse Boudouard Reforming (RDR), which utilizes methane cracking catalyst to supply H_2 for OC reduction, and the reverse Boudouard reaction to recover solid carbon from methane cracking into the CO product stream

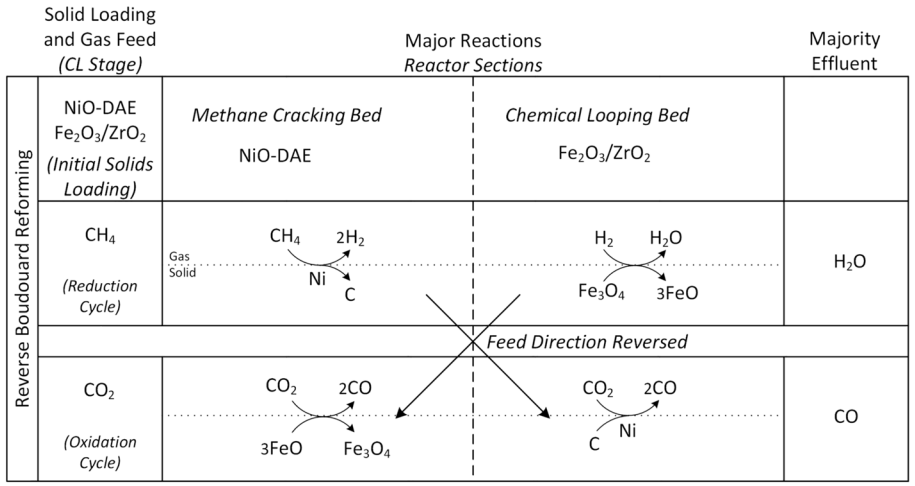

gas [7]. A variant using a co-feed of oxygen to achieve autothermal operation (ACACL) has also been suggested, with materials and process steps investigated by Hu [8] are summarized in Table 4. After initial pretreatment of metal oxide and support, the CL process is started by reducing the OC under H_2. Subsequent feed of CH_4, CO_2, O_2 mixture during the oxidation phase constitutes the autothermal production phase of the process. The dry reforming activity in the bed produces CO from CH_4 and CO_2, and CO production is intensified by the reducing activity of the metal oxide OC. A small co-feed of oxygen combusts CH_4 and H_2 in the system to offset the endothermic dry reforming reaction, allowing for autothermal operation of the bed.

2.3.4 Reverse Boudouard reforming (RBR)

The Reverse Boudouard Reforming (RBR) process utilizes a staged bed of two sections, loaded with methane cracking catalyt, and a metal oxide OC. Materials and configuration investigated by Keller[9] are summarized in Table 5. During the reduction stage, CH_4 is fed into the methane cracking bed, where $C_{(s)}$ and H_2 gas are produced. These gases proceed to the OC bed, where H_2 gas reduces the metal oxid. Gas feed direction is then switched, and feed gas changed to CO_2, which enters the CL bed first, and is converted to CO. Unreacted CO_2 exiting the CL bed then proceeds to the methane cracking bed, where CO_2 and $C_{(s)}$ combine to produce CO by the reverse Boudouard reaction.

2.4 Pathways comparison and placement

As the CO2CL pathways further evolve and specialize, their applications and most economic placement will consequently diversify. However, all the of the CO2CL pathways discussed here are closely linked in their chemistry, and historical development. These processes share the use of metal oxide structures to aid in the extraction of oxygen from highly stable H_2O and CO_2 molecules by incorporating the formation energies of the metal oxide ionic solids in oxygen transfer. The resulting product is one or both primary components of syngas (i.e., CO and H_2) for use in synthesis pathways in the materials economy. In all cases, significant energy input is required due to the high temperature of the process. Reductions in the required operating temperature have been realized by the incorporation of reducing gases (i.e., CH_4 and H_2), however the advantage of lower energy demand is offset by the cost of these new feedstocks.

Solar-concentrator powered reactors limit STCL to areas with high and consistent solar power densities at ground level. RWGS-CL sidesteps the requirement for solar concentrator reactors, but at the cost of H_2 demand. If sustainable versions of RWGS-CL are sought, the primary source of H_2 would likely be renewable energy fueled electrolysis. The placement of a sustainable RWGS-CL process would therefore have to be within range of large amounts of renewable energy (e.g., wind, solar, etc.). RWGS-CL usage of renewable H_2 could constitute an off-demand usage of renewable energy, allowing off-peak power production to be directed into H_2 generation by hydrolysis, for later use in mitigating CO_2 emissions from natural gas power production when local electrical demands are at peak capacity.

In the case of CLR, the abundance of natural gas following the fracking revolution in the United States makes CLR initially attractive for co-location with natural gas power generating facilities. With the power plant already having a CH_4 supply chain structure, and generating CO_2 in large quantities, the feedstocks for CLR are present in abundance at present power generation sites.

In all cases of CO2CL, the design of the OC material is paramount to maximizing production over chemical looping cycles. We further delve into a description of these oxygen carrier (OC) materials, and the course of their historical development.

3 Oxygen carrier materials and historical development

Candidate materials for these reactions are typically transition metal oxides and mixed metal oxides like perovskites and spinels, which have tunable surface and bulk chemistries through the incorporation of substitutional defects (i.e. different metal or molecular ions occupying lattice sites). Design of these OC materials by calculation of material stability while oxygen deficient has led to formulations which vastly increase the extent of oxygen deficiency the OC is capable of achieving under fixed reduction conditions (Table 6). The OC materials maintain stability under increasing oxygen deficiency by a number of mechanisms, including forming associates between defects [10, 11], diffusion of defects within the bulk structure [12], and local or bulk phases changes into metal oxide species [13] that differ as the extent of oxygen deficiency varies across the chemical looping cycle. High extent of reaction for the reduction phase and kinetics

Table 6 Performance of candidate materials for CO_2CL processes

Name	Type	CL process	Reaction temperature (°C)	CO yield (mmol/g_{OC})	References
CeO_2	Binary oxides	STCL	1400	0.25	[14, 15]
		RWGS-CL	1000	1.5	[16]
		CLR	800	–	[17, 18]
NiO	Binary oxides	CLR	950	–	[19]
Fe_2O_3/Fe_3O_4	Binary oxides	CLR	1200	0.12	[20]
CuO	Binary oxides	CLR	800	0.77	[21]
Fe_3O_4	Binary oxides	STCL	1400	0.27	[13, 22, 23]
SnO_2	Binary oxides	STCL	1600	–	[24]
ZnO	Binary oxides	STCL	1600	–	[25, 26]
$Sr_{0.6}La_{0.4}Mn_{0.6}Al_{0.4}O_{3-\delta}$	Perovskite oxides	STCL	1000	0.14	[27]
$Fe_{0.35}Ni_{0.65}O_x$	Spinel oxides	STCL	1400	0.17	[28]
$Fe_{0.45}Co_{0.55}O_x$	Spinel oxides	STCL	1400	0.09	[28]
$La_{0.4}Sr_{0.6}Mn_{0.4}Al_{0.6}O_3$	Perovskite oxides	STCL	1050	0.13	[29]
$La_{0.6}Sr_{0.4}Mn_{0.6}Al_{0.4}O_3$	Perovskite oxides	STCL	1050	0.25	[29]
$La_{0.5}Sr_{0.5}MnO_3$	Perovskite oxides	STCL	1050	0.22	[30]
$La_{0.5}Ba_{0.5}FeO_3$	Perovskite oxides	RWGS-CL	500	0.20	[4]
$LaCo_{0.25}Fe_{0.5}Mn_{0.25}FeO_3$	Perovskite oxides	RWGS-CL	600	0.90	[31]
$La_{0.75}Sr_{0.25}FeO_3$	Perovskite oxides	RWGS-CL	600	1.50	[32]
$La_{0.75}Sr_{0.25}FeO_3$ / SiO_2	Perovskite oxides	RWGS-CL	600	0.65	[33]
$La_{0.75}Sr_{0.25}FeO_3$ / SBA-15	Perovskite oxides	RWGS-CL	700	1.75	[34]
Co_3O_4 / $La_{0.75}Sr_{0.25}FeO_3$	Spinel oxides	RWGS-CL	600	1.15	[35]
Co-In_2O_3	Metal supported	RWGS-CL	500	1.64	[36]
6% K/BaFeHAl	Metal supported	RWGS-CL	550	0.38	[37]
Fe_2O_3-ZrO_2	Binary oxides	RWGS-CL	650	0.69	[38]
CeO_2	Ceria	STCLR	1050	2.16	[2]
$La_{0.95}Cu_{0.05}FeO_3$	Perovskite Oxide	CACL	850	2.28	[39]
Ni/CeO2-FeO3	Bifunctional MO	CACL	700	1.9	[7]
Cu-ZnO-Al_2O_3	Bifunctional MO	RBR	850	5.0	[9]

of the OC reduction and subsequent oxygen scavenging from CO_2 (a low severity oxidant), hold the key to efficient CL reactions for the OC oxidation step. To constrain the material design, a given reduction condition must be chosen for the development of an OC, which distinguishes different CO2CL processes.

The CO2CL process takes the OC through a cycle which swings in non-stoichiometric oxygen deficiency at elevated temperature. Suitable materials for the process must therefore have high stability across a region of oxygen composition, in contrast to steady state catalytic processes, where a material may be frozen in a particular defect or crystal geometry configuration to best serve kinetic and selectivity outcomes. In addition to thermodynamic stability, the OC must maintain a stable microscopic morphology over many cycles of CL. Significant sintering, agglomeration, or metal species migration within the OC over time has the potential to alter available surface area and surface composition for the heterogeneous reactions of the reduction and oxidation steps. In processes where oxygen vacancies are able to diffuse through the bulk, the length scale of the OC crystallites has a significant effect on time to complete a given extent of reduction or oxidation.

A large range of materials have been used till date—from well-known ceria-zirconia materials to state-of-the-art mixed metal oxides like perovskites or spinel oxides, as shown in Table 6. The material property of these oxides differs in terms of oxygen storage capacity, thermodynamic constraints for redox transformations, phase transition behavior, and internal oxygen diffusion characteristics.

However, the OC materials for CO2CL do share common characteristics: (1) They are ionic solids, with most bonds in the solid having predominantly ionic character over covalent, with nearly full electron transfer between atoms (2) They contain oxygen anions (3) Metal centers (typically transition metals) are present which are capable of multiple oxidation

states, allowing local electron transfer to accommodate the effective charge of vacancies. These features are all central to the OC's ability to maintain structural stability in the lattice when transitioning between different extents of oxygen deficiency. When an oxygen is removed from a lattice site, electroneutrality of the overall solid can be maintained by electron transfer to transitional metal centers, which undergo redox reaction. In a covalent material, the loss of a coordination site would necessarily result in an alteration in connectivity and structure. However, in the ionic solid, several mechanisms are present which may counteract the increased energy of the solid upon loss of a constituent oxygen anion. Local distortions of the crystal lattice may take place, moving remaining cations and anions to charge compensate the oxygen vacancy defect and the charge defect of the transition metal center which received electrons. At high temperatures, these materials exhibit substitutional defects which occur in equilibrium, including the established Schottky and Frenkel defect pairs. Diffusion of these defects allows them to coordinate with the oxygen vacancy defect, and accomplish charge compensation by associating defects with opposite signs of effective charge. Additionally, local changes in phase can take place, in which the crystal structure is altered to a new motif, with local charges and stoichiometry no longer matching the parent structure (analogous to a metal oxide transitioning from Fe_3O_4 to FeO). In this case, while the CO2CL chemistry may remain reversible, atomic and even microscopic rearrangement may occur over many cycles, leading to reduction resistant species, and sintering effects altering surface area and diffusion timescales. A tradeoff in material design is therefore struck between a formulation that is flexible, allowing for rapid diffusion of defects, and one that rigid in its thermodynamically preferred crystal structure.

Substitutional defects introduced in the material stoichiometry are the primary tool for altering the prevalence of the system for adsorption, dissociative adsorption (if necessary), and diffusion of oxygen vacancies between the bulk and surface. However, distribution of the substitutional (atom exchange) defects are not completely under the control of the experimenter by stoichiometric formulation. For example, swapping some of the A-site cations in the perovskite oxide $LaFeO_3$ for Ba (resulting in a formula $La_{(x)}Ba_{(1-x)}FeO_3$), does not produce a solid with homogeneous Ba composition throughout the solid. It has been observed that the surface becomes Ba enriched [4, 40–42], indicating the system thermodynamically favors the placement of Ba cations at the A-site on the surface over La cations. Diffusion of atoms between lattice sites at process temperatures may therefore place limits on the degree of control over local composition under certain formulations, as the alteration of local crystal composition may aid or hinder individual steps in the reduction and oxidation mechanism.

3.1 Course of material development

Early investigations into candidate materials for OC's were focused on metal oxides, and gradually moved to more complex structures like perovskites and spinels. The development course also incorporated reduction gases (in the cases of RWGS-CL and CLR) primarily aimed at reducing the required reaction temperature. The development of these materials brings to light their advantages and disadvantages.

3.1.1 Generation 1. metal oxidate material for solar thermochemical CO_2 to CO reaction

The thermochemical redox cycles generally operate in two separate steps, reduction and oxidation, utilizing a metal oxidate material (MO) as a reactive intermediate. For Fe_3O_4, the redox steps are shown in Eqs. (6) and (7) [43, 44]. The first thermal reduction step requires high energy input in reaction (1) (generally greater than 1200 °C), which is highly endothermic ($\Delta H^{o}_{298K} = 319.5$ kJ/mol). In the second step, the reduced oxide is reacted with H_2O and CO_2 at a lower temperature to produce H_2 and CO [45].

$$Fe_3O_4 \rightarrow 3FeO + 0.5O_2 \tag{6}$$

$$6FeO + CO_2 + H_2O \rightarrow 2Fe_3O_4 + CO + H_2 \tag{7}$$

Due to the extremely high-temperature requirement for the reduction, the category of metal oxide is divided to volatile and non-volatile materials (Table 7). For volatile materials, such as ZnO, the metal oxide can undergo significant gas–solid phase transitions at high temperatures in the reduction step [46]. For non-volatile materials, such as Fe_3O_4, the metal oxide material remains in the solid state during the reduction [47]. Generally, volatile materials produce more O_2 in the reduction step than non-volatile, which potentially converting more CO_2 to CO at the oxidation step, at the cost of potentially emitting metals from the reactor. To enhance the conversion yield of non-volatile materials, it is possible

Table 7 Common volatile and non-volatile metal oxide materials for thermochemical CO_2 to CO conversion

Category	Materials	Reduction reaction	References
Volatile	SnO_2	SnO_2 (s) → SnO (g) + ½ O_2	[25, 26]
	ZnO	ZnO (s) → Zn (g) + ½ O_2	[24]
Non-Volatile	Fe_3O_4	Fe_3O_4 (s) → 3FeO (s) + ½ O_2	[13, 22, 23]
	CeO_2	CeO_2 (s) → CeO (s) + ½ O_2	[14, 15]
	Perovskite oxides (ABO_3)	ABO_3 (s) → ABO_{3-x} (s) + x/2 O_2	[27, 49]

to increase the reaction temperature to force the reaction to the volatile process. For example, the thermal reduction to FeO requires temperatures above the melting point of both FeO (1377 °C) and Fe_3O_4 (1597 °C), the Fe_2O_3 converts to FeO at 1700 °C in 2 min for a single pellet of metal oxide in a solar concentrator reactor [48].

Although the thermochemical reaction successfully converts CO_2 to CO, the extremely high-temperature requirement in the reduction step is a major drawback limiting further its application. One method to develop the reaction is to use solar energy as the energy source to lower the costs [50]. However, a materials challenge induced by such high reduction temperatures is sintering. Methods such as mechanical crushing or milling for material regeneration. These limitations lead to the alteration of composition within stable crystal structures to influence reaction mechanisms.

3.1.2 Generation 2. Spinel substituted metal oxide for thermochemical CO_2 to CO reaction

Due to the challenge of the high energy requirement for thermochemical CO_2 to CO reaction, several optimized materials have been developed to lower the reaction temperature. One series of optimized materials is spinel substituted iron oxide ($Fe_{3-x}A_xO_4$ (A = Mn, Co, Ni, Zn)). The reduction behavior in the ferrite redox system can be influenced by partial cation substitution of Fe in the spinel. The spinel substituted iron oxide can reduce the reaction temperature by > 100 °C (650–1100 °C). Similarly, spinel substituted perovskite oxide materials could also reduce the energy requirement for the reduction. The common materials and their conversion properties are shown in Table 8.

3.1.3 Generation 3. Metal oxide material for CO_2 to CO reaction through RWGS-CL

To excise oxygen anions from the formulated spinels and perovskites at lower temperature, a reduction gas is introduced. The use of H_2 results in a leaving gas of H_2O rather than oxygen, lowering the net change in Gibbs energy, and therefore increasing equilibrium reduction at lower temperatures. The similarity to the established water gas shift (WGS) reaction led to the description of this process as RWGS-CL. The first step in RWGS-CL is to reduce the metal oxide material by H_2, forming the material with oxygen-vacancy (3). The second step is to oxidize reduced metal oxide by donating O from CO_2, producing the original metal oxide structure and CO (4).

$$MO_x + \delta H_2 \rightarrow MO_{x-\delta} + \delta H_2O \tag{8}$$

$$MO_{x-\delta} + \delta CO_2 \rightarrow MO_x + \delta CO \tag{9}$$

where MO_x represents a metal oxide and $MO_{x-\delta}$ represents a reduced metal oxide. Several perovskite oxide materials, including those supported on porous, inert oxides, are shown in Table 9.

The further developments of RWGS-CL materials can be focused on improving the materials properties in CO_2 to CO conversion, such as synthesizing the high surface area metal oxides and improving the dispersion by adding support material.

3.2 CLR materials

The development of chemical looping approaches to reforming (in this paper broadly referred to as CLR) were originally driven by the development of POM processes to limit the complete oxidation of CH_4 into CO_2 during syngas production. By incorporating an OC, the thermodynamics driving the oxidation of CH_4 through the desired product of CO and into the terminal combustion product of CO_2 could be modified. The OC for CLR is therefore responsible for transferring oxygen to an adsorbed CH_4 molecule, to produce CO and H_2O in the reduction step. As OC's for CLR developed, and interest in

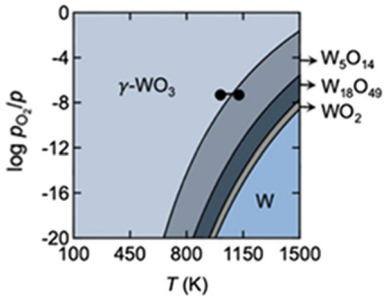

Fig. 6 Equilibrium O_2 partial pressure of metal oxides as a guiding tool for their use in chemical looping processes at desired reaction temperatures. A higher partial pressure of O_2 at equilibrium indicates a greater capacity for the solid to accommodate oxygen deficiency. (figure reproduced with permission from American Chemical Society [58])

CO_2 emission mitigation increased, OC's for CLR were developed to use CO_2 as the oxidation gas. Certain configurations of CLR have the potential to create CO in both steps of its CL cycle, from CO_2 in the oxidation step, and from CH_4 in the reduction step.

The need to activate CH_4 in CLR leads to different material formulations than those found in STCL and RWGS-CL. While the spinels and high temperature stable ionic solids common in other CL pathways are used in CLR, metal promoters such as Ni, Mn, and Co are used for their reforming chemistry and stability[54]. The primary metrics for a POM OC's are CH_4 conversion and CO selectivity (over CO_2 in the reduction step). In adapting the process to using CO_2 as the oxidizing gas, a further performance constraint is added in the ability of the OC to receive oxygen from the relatively weak oxidizing agent of CO_2. It is here that perovskite oxides enter again, in the familiar form of transition metal containing perovskite oxides acting as OC, and also capable of CH_4 activation [55]. With the incorporation of perovskite oxides and mixed metal oxides, the transition metals applicable to high performance in CLR is broadened to Ni, Cu, Fe, Mn, and Co [56].

3.3 Thermodynamics

The chemical looping process of CO_2 conversion revolves around redox cycling of OC by varying non-stoichiometric oxygen deficiency. The equilibrium extent of OC reduction at a given temperature and reducing gas partial pressure dictates upper limit of CO_2 conversion per cycle, which is ultimately a thermodynamic limit. Theoretical calculations to investigate phase changes are important to explore the oxygen exchange capacity (or more conventionally, oxygen storage capacity). Phase diagrams and/or Ellingham diagrams are helpful in illustrating the stability of metal oxides under different oxygen partial pressure, and reaction-relevant temperatures (Fig. 6). A greater equilibrium partial pressure of O_2 maintained by the OC indicates a greater capacity for the solid to reversibly accommodate oxygen deficiency within its structure, which directly impacts the amount of oxygen that can be transferred in a single CL cycle.

Expanding from the reduction pathway to the process as a whole, iron oxide processes for CO2CL (both with and without reducing gases) have been thermodynamically modelled to investigate energy requirements for CO production [57].

Phase stability studies on Mn–Fe–O systems [59] have elucidated the role of Mn-content on the redox capacity of these materials at 850–950 °C. The extent of reducibility of materials as studied via phase diagrams has led to the computational discovery of materials for chemical looping H_2 production [60]. Ab-initio investigation of phase diagrams are not only useful to predict the most stable bulk phases, but they can also provide insights into the most stable surface terminations and facets. For example, Zasada et al. have shown how reaction conditions dictate the surface structure of Co_3O_4 spinel oxides [61]. The specific surface termination in abundance sets the stage for the process by dictating the possible adsorbed species intermediates and adsorption energies for the gas–solid interface. The energy of oxygen vacancies in the lattice also differs between not only bulk and surface states, but also between different surface terminations, therefore altering the availability of oxygen vacancies at the surface as predicted by statistical mechanics models. Thermodynamically favored surface terminations can vary widely across process relevant temperatures, as shown in Fig. 7 for spinel structures. While each formulation of OC will vary in its surface termination in response to the temperature, this feature of the ionic solids relevant to CL processes introduces a complication to the development of kinetic models. As the high mobility of vacancies and defects within these solids at process temperatures allows the reconfiguring of their surface, the conditions for reaction mechanism steps (e.g.

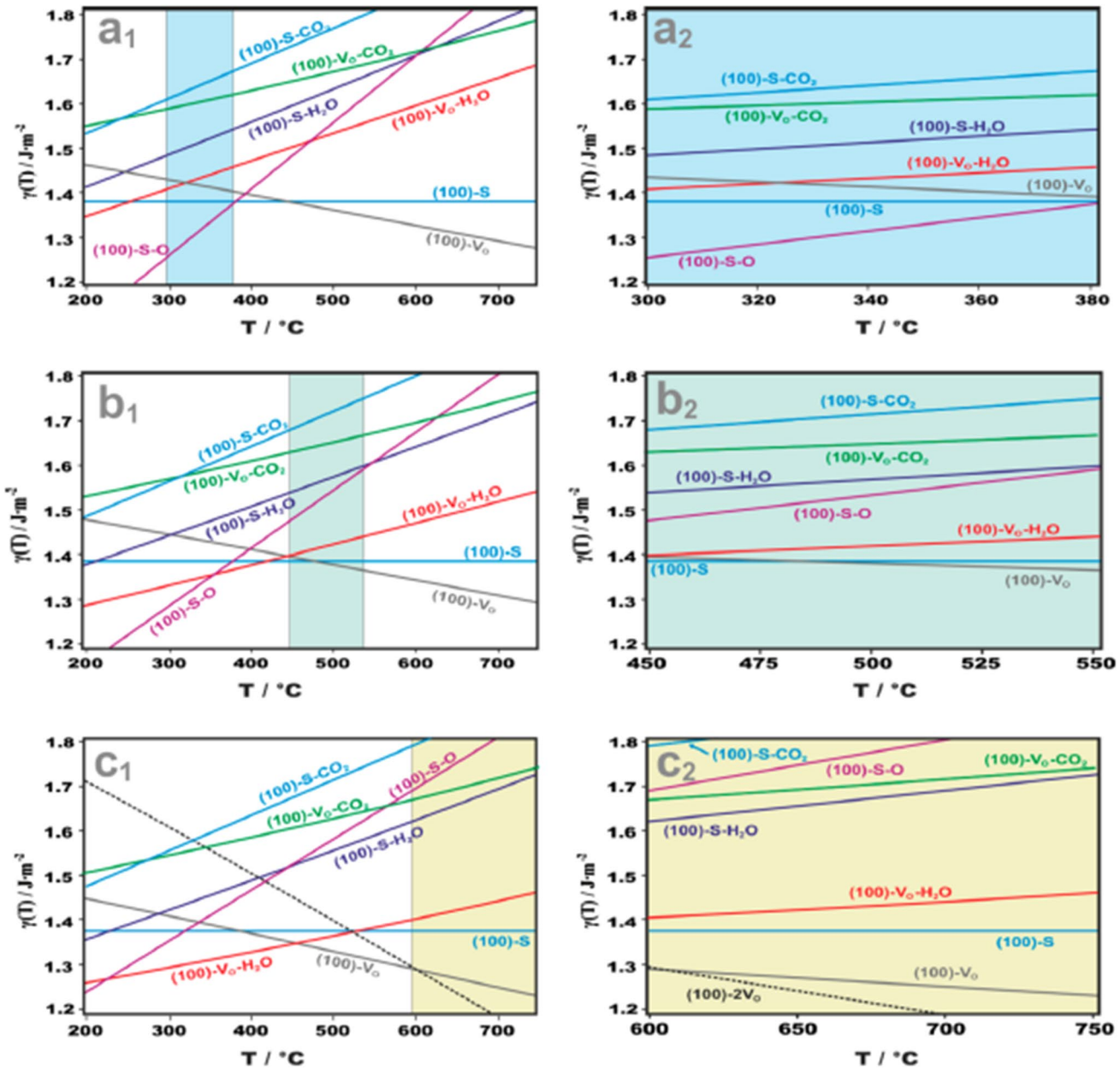

Fig. 7 Zasada et. al used first principles calculations to identify the most stable surface terminations of Co_3O_4 spinel oxides under appropriate reaction environment. The most stable surface state changes from a stoichiometric form (a1, a2) to an oxygen deficient state (b1, b2) to a more reduced surface (c1, c2) as the CH_4 conversion increases with temperature. (Reproduced with permission from the American Chemical Society [61])

adsorption, vacancy formation, etc.) at the surface may change significantly. As a result, the energy change associated with a given mechanistic step may be a function of temperature, violating simple Arrhenius rate laws.

Quantum chemical calculations, primarily based on DFT methods, have been used to probe the thermodynamic properties of these materials [62]. The vast range of complex mixed metal oxides being studied for these CL reactions is linked to successful prediction of metal compositions with CO_2 conversion abilities [3]. These are primarily descriptor-based efforts based on oxygen-vacancy formation energies, enthalpy of formation, band gap, atom-projected electronic density of states, appropriate for CO_2-conversion [63]. Oxygen vacancy formation energy (E_V) and enthalpy of formation of these oxides stand out as obvious choices for OC design criteria, as the chemical looping mechanism is intricately related to redox cycling of the materials. Ease of oxygen removal from a metal-oxide is thus a critical factor.

Table 8 Common spinel substituted metal oxide for thermochemical CO_2 to CO reaction

Materials	Reaction temperature (K)	CO yield (mmol/g_{cat})	References
$Ni_{0.5}Mn_{0.5}Fe_2O_4$	1073	–	[51, 52]
$Fe_{0.35}Ni_{0.65}O_x$	1673	0.17	[28]
$Fe_{0.45}Co_{0.55}O_x$	1673	0.09	[28]
$La_{0.4}Sr_{0.6}Mn_{0.4}Al_{0.6}O_3$	1323	0.13	[29]
$La_{0.6}Sr_{0.4}Mn_{0.6}Al_{0.4}O_3$	1323	0.25	[29]
$La_{0.5}Sr_{0.5}MnO_3$	1323	0.22	[30]

While large oxygen vacancy formation energy (E_V) corresponds to higher energy demand to break an oxygen atom free of the lattice, thus requiring higher temperatures for CL operation, too favorable oxygen vacancy formation (lower E_V) can result in so many vacancies that the crystal lattice collapses, resulting in irreversible phase changes in the OC. Thus, based on CL process needs, there is a fine balance of which materials can be used as redox platforms. These modeling efforts have proved to be useful for material property prediction, they stem from a static, thermodynamic perspective. More complete kinetic process descriptions require diffusion and reaction mechanisms, necessitating more expensive calculations.

3.4 Bulk and surface chemistry/defects

Mobility of defects between the surface and bulk is a major material property of interest in OC materials. In the absence of near molecular control over OC layer thickness on a catalyst substrate, diffusion of oxygen vacancy (and other charge compensating) defects allows the full bulk of the material to be utilized for oxygen cycling. Without significant defect diffusion, the oxygen cycling capacity will be fundamentally limited by the surface area of the OC. Increased concentration of surface bound defects will also increase the local strain on the lattice, potentially leading to phase changes, whereas an OC capable of distributing defects throughout its bulk will experience lower local strain, potentially delaying the onset of phase changes as reduction severity is increased.

Interchange of defects between bulk and surface of the OC also has a significant effect on the kinetics of the process. Even in the limiting case where the oxygen vacancy diffusion rate far exceeds the surface reaction rate, the distribution of defects between the surface and bulk will then be dictated by thermodynamics. As a result, the defects at the surface available for reaction will always be a fraction of the total defects within the solid. Without statistical mechanics correction, kinetic rate law parameters may be under estimated due to the over estimation of surface site (i.e. surface oxygen vacancies) concentration.

4 Reaction mechanisms

From a broad perspective, the minimum reaction steps during the CO2CL process are adsorption, surface reaction and solid reorganization, and desorption. There remains a lot of work to be done to elucidate the mechanistic steps of CO_2 conversion via CL techniques, and more importantly exploring the atomistic insights to design better solid reactants. The chemical looping approach to CO_2 reduction is based on a transient, dynamic evolution of the OC as the extent of oxygen deficiency changes over chemical looping steps. Most of the conventional catalyst performance metrics (percentage conversion, CO yield, conversion rates, TOF) for CL reaction scheme are either averaged over the cycle time or reported as the highest results per cycle. To have a better control of the reaction, and make the best of these dynamic reaction schemes, more detailed mechanistic investigations are required. During reduction/oxidation step, the solid reagent undergoes transitions/transformations in terms of oxidation state of metals [64, 65], varying reaction-available surface concentration of metals and oxygen [66], vacancy and crystal defects in varying forms [67], different metal-support interactions [33, 68], an ensemble of metal-oxide phases, crystal shapes and sizes, all having a significant effect on the electronic structure/state of the active sites [62, 67, 69, 70]. General characterization of new OC materials typically includes the use of XRD and TPR/TPO (Fig. 8). XRD is used to confirm the stability of the crystal structure across reaction conditions, or identify the formation of new phases. The example here shows the perovskite has maintained its crystal structure across the reduction and oxidation conditions, despite the evidence of stoichiometric loss of oxygen from

Table 9 Common materials for CO_2 to CO reaction through RWGS-CL

Materials	Reaction temperature (K)	CO yield (mmol/g_{cat})	References
$La_{0.5}Ba_{0.5}FeO_3$	773	0.20	[4]
$LaCo_{0.25}Fe_{0.5}Mn_{0.25}FeO_3$	873	0.90	[31]
$La_{0.75}Sr_{0.25}FeO_3$	873	1.50	[32]
$La_{0.75}Sr_{0.25}FeO_3/SiO_2$	873	0.65	[33]
$La_{0.75}Sr_{0.25}FeO_3$/SBA-15	973	1.75	[34]
$Co_3O_4/La_{0.75}Sr_{0.25}FeO_3$	873	1.15	[35]
Co-In_2O_3	773	1.64	[36]
6% K/BaFeHAl	823	0.38	[37]
Fe_2O_3-ZrO_2	923	0.69	[38]
$Mn_{0.2}Co_{0.8}Fe_2O_4$	923	8.80	[53]

the crystal. The TPR result (Fig. 8c) shows two major peaks for water emission. The evolution of water from 200-300C is common for perovskites, and considered to be mainly the loss of adsorbed species [4], which is convoluted with the water peak centered on 350C, which is ascribed to chemical reduction of the perovskite by generation of water. The TPO result (Fig. 8d) shows the production of CO from the reaction of CO_2 with oxygen deficient perovskite. The significant difference between the peak reduction and oxidation temperatures is driven by the severity of the reducing/oxidizing environment and stability of the products of the reaction. While these tools are crucial in verifying the bulk structure and general chemistry of the material formulation, they are unable to provide a detailed description of the changes in the OC across the CL cycle.

The XRD and integration of TPR/TPO results give indication of bulk changes to the perovskite or OC. However, local changes in defect concentration and association may occur at the surface, as well as distribute throughout the solid. As discussed in relation to Fig. 7, changing thermodynamic conditions has a large effect on the stability of surface configurations of defects, and surface terminations for the perfect crystal itself. As a result, the structure and configuration of active sites resulting in the desired reactions may change across thermodynamic regimes. XPS, DFT and other surface characterization or modeling techniques are required to gain insights into identifying the configuration of heterogeneous reaction sites.

4.1 Adsorption

For the operating temperatures of CO2CL processes, chemisorption is expected to dominate over physisorption, due to the larger adsorption energies required for persistent binding at high temperature. DFT studies have been carried out to identify stable adsorbed species. Even when idealized surfaces are simulated, candidates for intermediate species and adsorption sites vary depending upon the crystal termination plane, and stage of the chemical looping process.

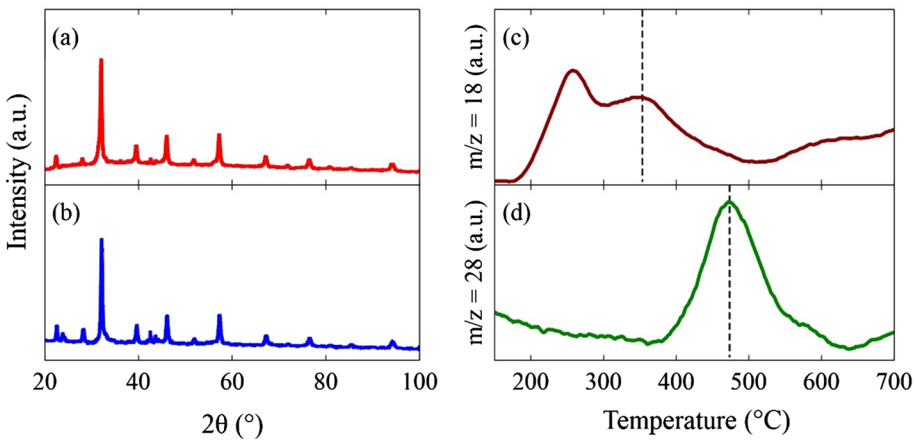

Fig. 8 Examples of material ($La_{0.5}Ba_{0.5}FeO_3$) characterization results. XRD results are used to confirm the formation of the expected crystal structure. TPR and TPO under the relevant reduction and oxidation gases reveal the onset of significant reactivity. **a** XRD result of fresh LBF, **b** XRD result of post-CL LBF, **c** TPR-H_2 result, and **d** TPO-CO_2 result. (Reproduced with permission from Elsevier [4])

For example, in the case of RWGS-CL oxidation step, DFT studies have revealed carbonate (CO_3) as a stable adsorption species with an incoming CO_2 gas molecule chemisorbing to an oxygen in the solid lattice [71]. Presence of carbonate is also corroborated by DRIFTS measurements over the same reaction step [4, 72]. However, the DFT studies indicate that the formation energy for the same carbonate species at an exposed oxygen site varies based upon the crystal surface termination plane. Accurate prediction of the adsorption rate from adsorption energies would therefore require a quantification of relative amounts of crystal termination area across the solid. The same complication arises when attempting to kinetically model the surface reaction and desorption rates, leading to the application of power law and equilibrium modified kinetic models [73].

4.2 Surface reaction and solid reorganization

Once a gas molecule has adsorbed at an appropriate site, a surface reaction and solid reorganization must occur for the reaction to proceed. It is unclear from experimental studies if the surface reaction is distinguishable from a desorption step, in which an oxygen atom exchanges between the OC and gas phase species. Ionic solid electroneutrality requires the redox induced restructuring (and a subsequent altering of effective charge) of elements within the solid OC to allow the transfer of oxygen anions to and from the OC. The redox reaction may be followed by the formation of point and extended defects within the same (or slightly distorted) crystal structure, or can result in the formation of new crystal phases within the OC. The manner in which the OC reorganizes to accommodate the change in extent of oxygen deficiency can therefore be distinguished by vacancy and phase change behavior.

4.3 Vacancy mediated oxygen carriers

Quantum mechanical simulation [10] and thermodynamic studies [11] coupled with experiment on oxygen deficient perovskites have indicated the redox primarily occurs at transition metal sites within the OC. Further, these studies also come to the same conclusion that the reduced transition metal sites and oxygen vacancies within perovskites are strongly correlated, and exist as associates of defects (also referred to as complexes or extended defects). In perovskites, the oxygen vacancies are highly mobile, allowing them to distribute throughout the bulk of the crystal structure following their formation on the surface through heterogenous reaction with the reactant gases. The extent of oxygen vacancy at the surface of the OC, and the relative rate of the diffusion of these vacancies relative to the rate of surface reaction result in a changing electronic environment on the surface of the OC. Since reaction is inherently governed/dictated by electronic interactions, this transient evolution of the solid surface impacts the CL performance as well. Starting with detailed ab-initio studies towards developing detailed microkinetic mapping of the reaction pathway and operando spectroscopic studies can lead to explore the dynamic behavior of these reactions. Ab-initio calculations to discover new material formulations have also been conducted to enable increased performances (e.g. oxygen vacancy formation energy) and validated by experiment (CO production per CL cycle) (Fig. 9 [66]). The general tunability of perovskites is demonstrated here, with fractional substitutions of A and B sites in the ABO3 structure altering the oxygen vacancy formation energy.

4.4 Phase mediated oxygen carriers

In the case of phase mediated OC, the reduction of metal centers results in reorganization of the solid to a new crystal structure geometry and/or local stoichiometry. The bulk diffusion of altered local phases is expected to be less than that of smaller extended defects, from the perspective of activated transport of the complete phase. However, reorganization of individual atoms at the boundaries between phases may result in the apparent motion of phases between the bulk and surface of the OC, in a process that is analogous, but more complex, than that of the diffusion of point defects and extended defects still occupying the original crystal lattice geometry. Issues of transport of altered phases, and morphological alterations such as sintering and grain boundary formation are of critical importance to maintaining CO2CL performance across many cycles for phase mediated OC.

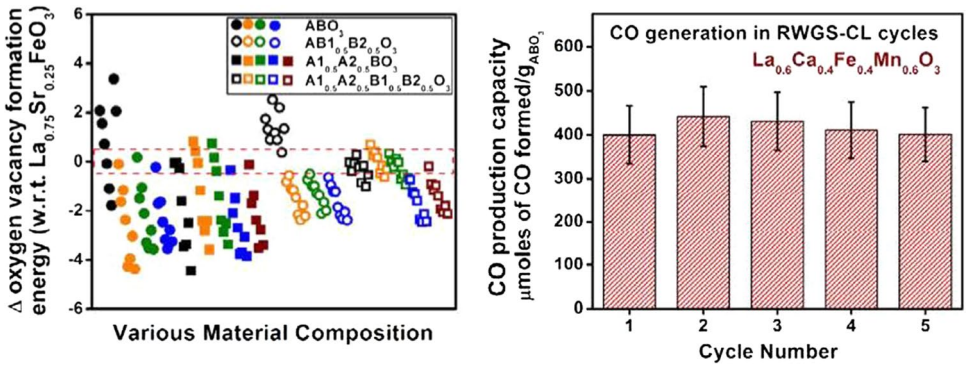

Fig. 9 Discovery of Earth-abundant perovskite oxides for CO_2 conversion by reverse water gas shift chemical looping (RWGS-CL) process by theoretical material calculations followed by experimental verification. Screened materials include perovskite composed with: A-site cations of La, Ba, and Ca; B-site cations of Cr, Mn, Fe, and Al. Ab-initio materials modeling of oxygen vacancy formation energy (**A**), normalized by property of reference material $La_{0.75}Sr_{0.25}FeO_3$. Experimental performance of CO production across serial CL cycles (**B**) for candidate material from theoretical search. Ab-initio oxygen vacancy formation energies were used as descriptors for the design search. (Reproduced with permission from the Royal Society of Chemistry [66])

4.5 Perspective on reaction mechanism development

Major performance features for OC in CL processes have been identified, here shown for the CLR process (Fig. 10). From the perspective of reactor design, larger conversion per unit of reactor volume decreases the frequency of cycling between reduction and oxidation stages. To this end, the utilization of the OC centers around its fundamental Oxygen Carrying Capacity (i.e. how much oxygen can be reversibly removed from the structure), Bulk Diffusion of defects to access the internal bulk of the OC, and sintering resistance to prevent mounting mass diffusion resistance. The reactor performance is also linked to the Surface Reaction rate, allowing higher WHSV, and selectivity for targeting high value products. As such, the material design process will of course benefit from a detailed understanding of the mechanism for the given CO2CL process.

As a function of timescale of reaction, and the allowed phase transformation under appropriate reaction environment, detailed microkinetic investigations are needed to capture the dynamic formation of reduced states (phases, or surface elements, and/or oxygen vacancies) and CO_2 activation as well. Dynamic phase transition is another key element. Ab-initio Ellingham diagrams [59, 69, 75] are great to showcase the phase evolution under reaction conditions. These studies can elaborate on the extent of material reduction from lattice oxygen vacancies on surfaces, to bulk, and finally phase transformation to metallic phases. These thermodynamic insights need to be coupled with kinetic properties to have a much better understanding of the time-dependent CL processes. Dynamic oxygen storage capacity (DOSC) is such a parameter that provides insights on the materials' capacity for oxygen exchange [76–79] during each step of the CL process. Thus, a detailed description of oxygen diffusion kinetics and thermodynamic properties [74, 78] are required for the design of new OC materials. During the reduction step of CL, the surface lattice oxygens are the first ones to get depleted, which get replenished from the bulk. Materials like perovskite oxides with more open oxygen sublattices exhibit higher bulk-oxygen diffusivities [74]. These materials

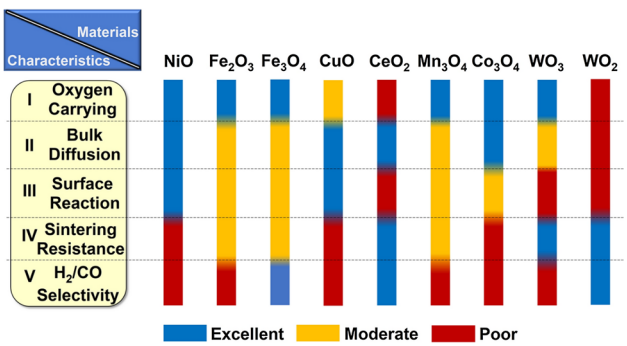

Fig. 10 Oxygen carrier development for chemical looping reforming process. (Reproduced with permission from Springer Nature [74])

thus allow faster bulk-to-surface oxygen transport and are more favorable for CL applications. Ab-initio oxygen diffusion barriers have been calculated. A combination of lower E_V, and oxygen diffusion barrier is desired for higher reduction of a material [80]. To delve into more intricate material crystal complexities, dynamic evolution of the surface states—charge states, spin states, selective surface segregation of elements, and vacancy configurations should be considered towards explaining the intrinsic reaction rates and activation barriers. Complexities involving mixed metal oxides are manifold as not only do they present several surface terminations with varying metal compositions, but the undercoordinated surface metals can also switch between coordination states, spin states, thus presenting a different electronic state from their bulk coordination environment [70]. Thus, more rigorous theoretical calculations coupled with operando studies are encouraged. While most theoretical studies are still involved in probing certain metal-reactant interactions, more holistic approaches involving coverage dependence, metal-vacancy dual sites, spillover mechanisms [81], can provide more reaction-relevant insights. These studies are not meant just to explore the mechanistic behavior but can also guide the design of dynamic CL operation towards maximum flexibility, energy-efficiency, and enhanced CO_2 conversion.

The role of operando studies cannot be ignored in the pursuit of intrinsic mechanistic insights, especially for a dynamic process. Operando investigation of variation of the crystal structure, charge states of the surface species, and site agglomeration, are critical in understanding the varying reaction rates. In-situ studies have shown the evolution and/or stability of the material phases over CL cycles [13, 67]. In-situ Raman spectroscopy studies are great to investigate the progression of CL reactions as oxygen non-stoichiometry evolves [82]. While post reaction characterizations showcase the evolution of surface metal concentrations [66] and metal-support interactions [68], rigorous operando studies are required to elaborate these material transformations. Vacancy defects, their concentration, and their charge states need to be explored. While it has been shown that CO_2 conversion increases with higher oxygen non-stoichiometry on perovskite oxides [3], operando studies are crucial for the purpose of elucidating the oxides' defect chemistry [83, 84] and CO_2 activation mechanism—a joint metal-Vo site driven activation, or CO_2 activation solely on metal, with subsequent O-spillover and diffusion to vacant sites. The site-specific mechanistic differences as a function of different reducing agents (heat, H_2, and CH_4) deserve special attention as well. Particularly the role of C-deposition during CL reforming needs to be probed towards exploring subsequent C–V_O mediated CO_2 activation. The lifetime of surface-active intermediates are important parameters as well. Isotopic labelling studies, along with pump-probe experiments in the Temporal Analysis of Products (TAP) reactor [85, 86] can provide specific insights on surface lifetimes [87] and intrinsic surface-state specific reaction rates [88], and oxygen exchange, instead of an ensemble average of varied reaction rates. TAP-studies with in-situ spectroscopic investigations can pave the way for providing such site-specific CO_2 activation rates. The intrinsic CO_2 conversion rates as a function of O-vacancy concentrations can be probed via state-defining experiments [89] in the TAP reactor. DFT-calculations along with these experimental approaches are pathways for unraveling the transient CL reaction mechanisms.

5 Reactor operations and scale-up

Reactor strategies for CO2CL require the separation of reduction and oxidation conditions for the oxygen storage material. These conditions can be separated in time using a single packed bed reactor, in which the feed gas or temperature is switched, or separated in space by using circulating fluidized bed reactors, in which one reactor operates at the reduction condition and the other at the oxidation condition. While the primary motivation for CO2CL over direct metal oxidation is the elimination of net production of metal oxides (and therefore the demand for reduced metal species), significant advantages in operational and equipment costs are also realized through simplified separations. In a catalytic process for CO2 to CO using OC materials, the product (CO) would be mixed with unreacted CO_2, as well as the gas phase products and reactants from the reduction reaction (H_2, H_2O, CH_4, O_2 etc.). Separating the reduction and oxidation steps in time or space eliminates contamination of the CO product by reduction reaction species, making acid gas adsorption for CO_2/CO separation a potential single step separation for product purification. Additionally, decoupling of product purity specification with recovery of unreacted reactants for recycle further reduces separation demand, as a plant may be able to tolerate more loss of reduction chemistry reactant in a stream that is not subject to downstream product purity constraints.

5.1 Reactor configuration: fixed and fluidized beds

While processes for CO2CL consisting of a cycling packed bed reactor (CPBR) or pair of circulating fluidized bed reactors (CFBR) may both reap the separations advantages of CL, there are significant tradeoffs in advantages and disadvantages between them [90].

A cycling packed bed reactor (CPBR) for CO2CL would consist of a reactor loaded with an OC on a pellet substrate to limit excessive pressure drop and maintain the mechanical integrity of the packing. The CPBR would be fed reduction gas, purged, then oxidation gas, and purged to complete one CL cycle. Effluent collection and purge systems would be switched over corresponding to the stage of reaction/purge within the reactor.

A pair of circulating fluidized bed reactors (CFBR) would consist of two fluidized bed reactors with separate gas inlets and effluents, while circulating solids between them. The circulating solid would be an OC on a powder catalyst, of spherical geometry and mechanical resilience to undergo the fluidization and cyclone separation of gas/solid without significant attrition. Each reactor would operate continuously, with reduction of the OC occurring in one fluidized bed, and oxidation in the other. Each reactor effluent would be continuously routed to the relevant product separation and recovery system.

Operation of the CPBR is fundamentally simpler than maintaining the CFBR, but at the cost of semi-batch in the packed configuration (fixed inventory of OC, continuous gas feed) instead of the continuous operation of the fluidized configuration. Capital cost of the CFBR configuration is also increased due to the requirement of cyclones for separating process gas from the fluidized bed solids. However, commercial advantage despite increased cost of capital expenditure and complexity of operation in CFBR has been demonstrated at scale in FCC. FCC is a catalytic process, but one in which a coke byproduct forms on the catalyst that rapidly diminishes process kinetics through site deactivation and transport resistance. While the mechanism of FCC deactivation through coke formation is different from the CO2CL process, the consumption of oxygen deficiency in OC occurs over similar timescales. In short, both processes utilize a solid in a heterogeneous reaction in which the solid rapidly loses its ability to react. The success of FCC at the highest industrial scales and the similarity in time scale of solids deactivation between FCC and CO2CL suggests the consideration of CFBR process configuration for CO2CL, and subsequently demands the refinement of kinetic modeling and substrate formulations for CO2CL over specific OC formulations to compare the process configurations of CPBR and CFBR. Despite incomplete understanding of mechanism steps, a variety of power law and equilibrium limited kinetic expressions have been developed [90], and applied to particular process configurations, and particle geometries for internal transport models [91, 92].

Wenzel et. al. [90] simulated RWGS-CL processes in a single PBR and FBR to evaluate the reactor design choice. The OSM utilized is Fe_2O_3-$Ce_{0.5}Zr_{0.5}O_2$, wherein the iron oxide undergoes a phase-mediated oxygen transfer, as evidenced by the construction of the rate laws utilizing equilibrium relationships between gas phase species and the various configurations of the iron oxides. Local advantages are found for conversion in the PBR design, where reaction fronts result in high gas partial pressures, while the FBR designs had higher performance near equilibrium conditions. Performance metrics were suggested to draw attention to these characteristics, including OSM Utilization, and average CO concentration.

5.2 Process efficiency and performance

Wenzel et al. [57]. investigated overall process efficiency for production of syngas from solar powered hydrolysis sources of renewable hydrogen, with a number of operating schemes involving conventional RWGS and RWGS-CL. The reactor operation for the RWGS-CL was a pair of CPBRs, which cycled between reduction and oxidation stages for the OSM. Quasi-steady state production is achieved through one reactor producing (oxidation stage) while the other is regenerated (reduction stage). Efficiency gains for the solar-to-syngas evaluation boundary were obtained primarily through heat integration, and the optimum H2/CO2 ratios identified for RWGS-CL which leveraged the already lower separation costs in CL processes over conventional catalytic systems.

Also investigating performance in RWGS-CL processes, Metcalfe et al. [93]. determined an information theory approach to tracking the state of oxygen deficiency in the OSM, coining the term "Memory Reactor" to describe the process of a reversible heterogeneous reaction wherein the solid remains captured in the bed. RWGS-CL was reported in this work

to exceed the equilibrium limit of conventional WGS/RWGS catalytic processes when the reaction quotient is calculated from the time-averaged reactor effluent concentrations over the reduction and oxidation stages of the CL process.

In the realm of solar thermal chemical processes, Bulfin et al. [94]. have developed and suggested non-dimensional performance metrics to allow for more rapid comparison on developing technologies and models. As pointed out in Wenzel's work [57], common system boundaries and definitions must be used for direct translation of performance metrics between investigations. Energy efficiency and reaction performances are defined, both for the well established 'thermochemical redox CO2 splitting' (in this work referred to as STCL), Solar Methane Reforming, and Biomass Gasification, as well as for any generic process utilizing solar energy to directly drive chemical processes.

In further extension of this work, extensive reactor modeling and experimental validation was carried out by Bulfin et al. [95] investigating the performance of RWGS-CL in a counter current, cycling fixed bed reactor, and comparing to conventional RWGS using a membrane reactor. As with their previous work, significant advantages in conversion and operating temperature were realized when utilizing CL rather than the catalytic process. The use of counter current (opposite flow directions of reduction and oxidation gases between stages) was justified on the grounds of maintaining a strong chemical potential difference over the reactor. As the reaction front proceeds through the OSM, a counter current arrangement keeps high concentrations of reagent gases in contact with sections of the bed where oxygen vacancies (or more general oxygen chemical potential) in the OSM are low, thus making better usage of the reactor volume in a concept analogous to maintain the log mean temperature difference in a counter current heat exchanger.

5.3 Reactor media

Substrate requirements for packed bed and fluidized bed reactors diverge in size, morphology, and mechanical properties, but share the necessity of large surface area and OC stability and adhesion over many CL cycles. Packed beds fundamentally require larger support geometries (0.5–5 cm) to prevent excessive pressure drop, while fluidized beds operate with small particles (50–200micron) that can be easily fluidized and separated from gas effluent by cyclones. In order to experimentally validate modeling efforts, candidate OC materials must be combined with reactor appropriate supports, beyond the pure and crushed materials generally used in micro-packed bed evaluations of particular OC formulations.

5.4 Conversion limits for defect and phase mediated ocs in cpbrs

Theoretical conversion limits at long times on stream (t_∞) in CPBR configurations of CO2CL differ based upon the OC being defect or phase mediated. For a CPBR, the t_∞ is defined as an extended period of time flowing the feed gas for the particular CL stage, long past the time when the desired product gas has ceased generation. In this scenario, calculation of the reaction quotient necessarily involves zero concentration (and therefore zero activity) of the product gas species. If the Gibbs energy of the reaction at present conditions predicts forward reaction, the absence of product gas would seemingly result in continued forward reaction. This is indeed the case with an OC operating on a phase mechanism, where a pure substance metal oxide is converted to reduced metal or a form of the metal oxide with a different oxidation state, and a theoretical complete conversion of the solid reagent (from the perspective of a single CL stage) is possible. In contrast, in defect mediated OC, an equilibrium limitation is met as the solid accumulates defects, which in the case of OC occurs primarily as substitutional defects in the form of oxygen vacancies.

The behavior of equilibrium limitation during the CL stage accumulating defects in the OC results from the Gibbs energy of the OC being a function of the oxygen deficiency (δ). DFT results have shown that oxygen vacancy formation energy increases linearly with increase of oxygen deficiency in perovskites for low to moderate oxygen deficiency [67]. As a result, the internal energy of the OC increases quadratically with mounting oxygen deficiency. The combinatorics component of the entropy of the solid decreases as the vacancy concentration increases, combining with the internal energy increase to drive up the Gibbs energy of the solid. As a result, in defect mediated OCs, the Gibbs energy of reaction for the reduction of the OC changes not just with temperature and pressure, but also with the oxygen deficiency. Sufficiently high oxygen deficiency will halt the OC by an equilibrium limit, even in the absence of product gas, as is the case for t_∞ in a CPBR. As a result, long run times for the reduction stage in a CPBR with phase mediated OCs can theoretically convert all OC to the reduced state, but defect mediated OCs cannot reach complete solids conversion under reduction conditions.

6 Summary and conclusions

While chemical looping technologies are an exciting pathway for CO_2 conversion into feedstock for fuels and materials for sustainable carbon loops or carbon sequestration, the energy demand and reducing gas demand (where applicable) must still be met, likely by co-location with large CO_2 emitters, current natural gas pipelines or production areas, and renewable energy installations. Materials for high performance oxygen carriers (OC) from abundant metals have been identified, synthesized, and tested in small scale fixed bed reactors by a number of researchers. Further scaleup requires detailed kinetic models for the oxidation and reduction steps of the chemical looping process, and are likely to require state of the art tools such as TAP reactor studies. The development of OC's on suitable substrates for fixed or fluid bed operation is also required to increase the scale of reactor performance studies beyond that of sub-micron powders in fixed beds to validate the preliminary reactor modeling studies.

Author contributions Article Concept- CS, VR. B, JN. K. Literature Search—CS, HS, DM, BJ. H, VR. B, JN. K. Drafting and Critical Revision—CS, HS, DM, BJ. H, VR. B, JN. K.

Funding This study was partially funded by National Science Foundation grant and IIP-1913722, Florida High Tech Corridor, and a USF Fellowship (to HS).

Data availability Not applicable.

Code availability Not applicable.

Declarations

Competing interests Venkat R. Bhethanabotla, John N. Kuhn declare patents and other financial interests in this technology.

References

1. Haeussler A, et al. Non-stoichiometric redox active perovskite materials for solar thermochemical fuel production: A review. Catalysts. 2018;8(12):611.
2. Chuayboon S, Abanades S, Rodat S. Solar chemical looping reforming of methane combined with isothermal H2O/CO2 splitting using ceria oxygen carrier for syngas production. J Energy Chem. 2020;41:60–72.
3. Daza, Y.A., et al., *Isothermal reverse water gas shift chemical looping on La0. 75Sr0. 25Co (1– Y) FeYO3 perovskite-type oxides.* Catalysis Today, 2015. **258**: p. 691–698.
4. Shi, H., V.R. Bhethanabotla, and J.N. Kuhn, *Role of Ba in low temperature thermochemical conversion of carbon dioxide with LaFeO3 perovskite oxides.* Journal of CO2 Utilization, 2021. **51**: p. 101638.
5. Zhao Y, et al. Thermodynamic analysis of a new chemical looping process for syngas production with simultaneous CO2 capture and utilization. Energy Convers Manage. 2018;171:1685–96.
6. Buelens LC, et al. Super-dry reforming of methane intensifies CO2 utilization via Le Chatelier's principle. Science. 2016;354(6311):449–52.
7. Galvita VV, et al. Catalyst-assisted chemical looping for CO2 conversion to CO. Appl Catal B. 2015;164:184–91.
8. Hu, J., et al., *CO2 conversion to CO by auto-thermal catalyst-assisted chemical looping.* Journal of CO2 Utilization, 2016. **16**: p. 8–16.
9. Keller M, Sharma A. Reverse Boudouard reforming produces CO directly suitable for the production of methanol from CO2 and CH4. Chem Eng J. 2022;431: 134127.
10. Eichel R-A. Structural and dynamic properties of oxygen vacancies in perovskite oxides—analysis of defect chemistry by modern multi-frequency and pulsed EPR techniques. Phys Chem Chem Phys. 2011;13(2):368–84.
11. Van Roosmalen J, Cordfunke E. A new defect model to describe the oxygen deficiency in perovskite-type oxides. J Solid State Chem. 1991;93(1):212–9.
12. Cheng Z, et al. New insight into the development of oxygen carrier materials for chemical looping systems. Engineering. 2018;4(3):343–51.
13. Coker EN, et al. Ferrite-YSZ composites for solar thermochemical production of synthetic fuels: in operando characterization of CO2 reduction. J Mater Chem. 2011;21(29):10767–76.
14. Furler P, et al. Solar thermochemical CO_2 splitting utilizing a reticulated porous ceria redox system. Energy Fuels. 2012;26:7051–9.

15. Hao Y, Yang C-K, Haile SM. High-temperature isothermal chemical cycling for solar-driven fuel production. Phys Chem Chem Phys. 2013;15(40):17084–92.
16. Farooqui AE, et al. Assessment of kinetic model for ceria oxidation for chemical-looping CO2 dissociation. Chem Eng J. 2018;346:171–81.
17. Kiyoshi O, Tetsuya U, Ichiro Y. Partial Oxidation of Methane Using the Redox of Cerium Oxide. 1993;22(9):1517–20.
18. Zhu X, et al. Hydrogen and syngas production from two-step steam reforming of methane using CeO2 as oxygen carrier. J Nat Gas Chem. 2011;20(3):281–6.
19. Rydén M, Lyngfelt A, Mattisson T. Chemical-Looping Combustion and Chemical-Looping Reforming in a Circulating Fluidized-Bed Reactor Using Ni-Based Oxygen Carriers. Energy Fuels. 2008;22(4):2585–97.
20. Hossain MM, de Lasa HI. Chemical-looping combustion (CLC) for inherent CO2 separations—a review. Chem Eng Sci. 2008;63(18):4433–51.
21. Guo L, Zhao H, Zheng C. Synthesis gas generation by chemical-looping reforming of biomass with natural copper ore as oxygen carrier. Waste and Biomass Valorization. 2015;6(1):81–9.
22. Kodama T, Nakamuro Y, Mizuno T. A Two-Step Thermochemical Water Splitting by Iron-Oxide on Stabilized Zirconia. J SolEnergy Eng. 2004;128(1):3–7.
23. Gokon N, et al. Monoclinic zirconia-supported Fe3O4 for the two-step water-splitting thermochemical cycle at high thermal reduction temperatures of 1400–1600°C. Int J Hydrogen Energy. 2009;34(3):1208–17.
24. Abanades S, et al. Novel two-step SnO2/SnO water-splitting cycle for solar thermochemical production of hydrogen. Int J Hydrogen Energy. 2008;33(21):6021–30.
25. Perkins C, Lichty PR, Weimer AW. Thermal ZnO dissociation in a rapid aerosol reactor as part of a solar hydrogen production cycle. Int J Hydrogen Energy. 2008;33(2):499–510.
26. Loutzenhiser PG, Meier A, Steinfeld A. Review of the Two-Step H2O/CO2-Splitting Solar Thermochemical Cycle Based on Zn/ZnO Redox Reactions. Materials. 2010;3(11):4922–38.
27. McDaniel AH, et al. Sr- and Mn-doped LaAlO3−δ for solar thermochemical H2 and CO production. Energy Environ Sci. 2013;6(8):2424–8.
28. Zhai S, et al. High-capacity thermochemical CO2 dissociation using iron-poor ferrites. Energy Environ Sci. 2020;13(2):592–600.
29. Sastre, D., et al., *Exploring the Redox Behavior of La0.6Sr0.4Mn1−xAlxO3 Perovskites for CO2-Splitting in Thermochemical Cycles.* Topics in Catalysis, 2017. **60**(15): p. 1108–1118.
30. Demont A, Abanades S. High redox activity of Sr-substituted lanthanum manganite perovskites for two-step thermochemical dissociation of CO2. RSC Adv. 2014;4(97):54885–91.
31. Ramos AE, et al. Co, Fe, and Mn in La-perovskite oxides for low temperature thermochemical CO2 conversion. Catal Today. 2019;338:52–9.
32. Daza, Y.A., et al., *More Cu, more problems: Decreased CO_2 conversion ability by Cu-doped $La_{0.75}Sr_{0.25}FeO_3$ perovskite oxides.* Surface Science, 2016. **648**: p. 92–99.
33. Hare BJ, et al. Enhanced CO2 Conversion to CO by Silica-Supported Perovskite Oxides at Low Temperatures. ACS Catal. 2018;8(4):3021–9.
34. Brower JC, et al. Mesoporous Silica Supported Perovskite Oxides for Low Temperature Thermochemical CO2 Conversion. ChemCatChem. 2020;12(24):6317–28.
35. Lee M, et al. Reverse Water-Gas Shift Chemical Looping Using a Core-Shell Structured Perovskite Oxygen Carrier. Energies. 2020;13(20):5324.
36. Makiura J-I, et al. Efficient CO2 conversion to CO using chemical looping over Co–In oxide. Chem Commun. 2022;58(31):4837–40.
37. Utsis N, et al. Reverse Water Gas Shift by Chemical Looping with Iron-Substituted Hexaaluminate Catalysts. Catalysts. 2020;10(9):1082.
38. Wang B, et al. Oxygen-Vacancy-Activated CO2 Splitting over Amorphous Oxide Semiconductor Photocatalyst. ACS Catal. 2018;8(1):516–25.
39. Liao X, et al. Highly efficient reduction of O2-containing CO2 via chemical looping based on perovskite nanocomposites. Nano Energy. 2020;78: 105320.
40. Bhavani AG, Kim WY, Lee JS. Barium Substituted Lanthanum Manganite Perovskite for CO2 Reforming of Methane. ACS Catal. 2013;3(7):1537–44.
41. Wu X, et al. Nitrate storage behavior of Ba/MnOx–CeO2 catalyst and its activity for soot oxidation with heat transfer limitations. J Hazard Mater. 2010;181(1):722–8.
42. Peralta MA, et al. Stability of Ba, K/CeO2 catalyst during diesel soot combustion: Effect of temperature, water, and sulfur dioxide. J Catal. 2006;242(1):118–30.
43. Coker EN, Ambrosini A, Miller JE. Compositional and operational impacts on the thermochemical reduction of CO2 to CO by iron oxide/yttria-stabilized zirconia. RSC Adv. 2021;11(3):1493–502.
44. Kodama T, Gokon N. Thermochemical Cycles for High-Temperature Solar Hydrogen Production. Chem Rev. 2007;107(10):4048–77.
45. Scheffe JR, Steinfeld A. Oxygen exchange materials for solar thermochemical splitting of H2O and CO2: a review. Mater Today. 2014;17(7):341–8.
46. Steinfeld A. Solar hydrogen production via a two-step water-splitting thermochemical cycle based on Zn/ZnO redox reactions. Int J Hydrogen Energy. 2002;27(6):611–9.
47. Nakamura T. Hydrogen production from water utilizing solar heat at high temperatures. Sol Energy. 1977;19(5):467–75.
48. Charvin P, et al. Two-step water splitting thermochemical cycle based on iron oxide redox pair for solar hydrogen production. Energy. 2007;32(7):1124–33.
49. Scheffe JR, Weibel D, Steinfeld A. Lanthanum–Strontium–Manganese Perovskites as Redox Materials for Solar Thermochemical Splitting of H2O and CO2. Energy Fuels. 2013;27(8):4250–7.
50. Marxer D, et al. Solar thermochemical splitting of CO2 into separate streams of CO and O2 with high selectivity, stability, conversion, and efficiency. Energy Environ Sci. 2017;10(5):1142–9.
51. Tamaura Y, et al. Production of solar hydrogen by a novel, 2-step, water-splitting thermochemical cycle. Energy. 1995;20(4):325–30.
52. Tamaura Y, et al. Thermodynamic evaluation of water splitting by a cation-excessive (Ni, Mn) ferrite. Int J Hydrogen Energy. 1998;23(12):1185–91.
53. Jain A, et al. Commentary: The Materials Project: A materials genome approach to accelerating materials innovation. APL Mater. 2013;1(1):011002.
54. Adanez J, et al. Progress in chemical-looping combustion and reforming technologies. Prog Energy Combust Sci. 2012;38(2):215–82.
55. Rydén M, et al. Combined oxides as oxygen-carrier material for chemical-looping with oxygen uncoupling. Appl Energy. 2014;113:1924–32.

56. Tang M, Xu L, Fan M. Progress in oxygen carrier development of methane-based chemical-looping reforming: A review. Appl Energy. 2015;151:143–56.
57. Wenzel M, Rihko-Struckmann L, Sundmacher K. Thermodynamic analysis and optimization of RWGS processes for solar syngas production from CO2. AIChE J. 2017;63(1):15–22.
58. Lee Y-J, Lee T, Soon A. Phase stability diagrams of group 6 Magnéli oxides and their implications for photon-assisted applications. Chem Mater. 2019;31(11):4282–90.
59. Azimi G, et al. Investigation of different Mn–Fe oxides as oxygen carrier for chemical-looping with oxygen uncoupling (CLOU). Energy Fuels. 2013;27(1):367–77.
60. Rojas J, et al. Computational discovery of metal oxides for chemical looping hydrogen production. Cell Reports Physical Science. 2021;2(3): 100362.
61. Zasada F, et al. Total oxidation of lean methane over cobalt spinel nanocubes controlled by the self-adjusted redox state of the catalyst: experimental and theoretical account for interplay between the Langmuir-Hinshelwood and Mars-Van Krevelen mechanisms. ACS Catal. 2017;7(4):2853–67.
62. Sai Gautam, G., E.B. Stechel, and E.A. Carter, *Exploring Ca–Ce–M–O (M= 3d Transition Metal) Oxide Perovskites for Solar Thermochemical Applications.* Chemistry of Materials, 2020. **32**(23): p. 9964–9982.
63. Deml AM, et al. Tunable Oxygen Vacancy Formation Energetics in the Complex Perovskite Oxide Sr x La1–x Mn y Al1–y O3. Chem Mater. 2014;26(22):6595–602.
64. Scheffe JR, Steinfeld A. Thermodynamic analysis of cerium-based oxides for solar thermochemical fuel production. Energy Fuels. 2012;26(3):1928–36.
65. Muhich C, Steinfeld A. Principles of doping ceria for the solar thermochemical redox splitting of H 2 O and CO 2. Journal of Materials Chemistry A. 2017;5(30):15578–90.
66. Maiti D, et al. Earth abundant perovskite oxides for low temperature CO 2 conversion. Energy Environ Sci. 2018;11(3):648–59.
67. Maiti D, et al. Oxygen vacancy formation characteristics in the bulk and across different surface terminations of La (1–x) Sr x Fe (1– y) Co y O (3– δ) perovskite oxides for CO 2 conversion. Journal of Materials Chemistry A. 2016;4(14):5137–48.
68. Hare BJ, et al. Thermochemical conversion of carbon dioxide by reverse water-gas shift chemical looping using supported perovskite oxides. Catal Today. 2019;323:225–32.
69. Zeng L, et al. Metal oxide redox chemistry for chemical looping processes. Nat Rev Chem. 2018;2(11):349–64.
70. Trottier RM, et al. Predicting Spinel Disorder and Its Effect on Oxygen Transport Kinetics in Hercynite. ACS Appl Mater Interfaces. 2020;12(21):23831–43.
71. Hammami R, Batis H, Minot C. Combined experimental and theoretical investigation of the CO2 adsorption on LaMnO3+y perovskite oxide. Surf Sci. 2009;603(20):3057–67.
72. Shi, H., V.R. Bhethanabotla, and J.N. Kuhn, *Pelletized SiO2-supported La0.5Ba0.5FeO3 for conversion of CO2 to CO by a reverse water-gas shift chemical looping process.* Journal of Industrial and Engineering Chemistry, 2022.
73. Wenzel, M., et al., *CO production from CO2 via reverse water–gas shift reaction performed in a chemical looping mode: Kinetics on modified iron oxide.* Journal of CO2 Utilization, 2017. **17**: p. 60–68.
74. Zheng H, et al. Chemical looping reforming: process fundamentals and oxygen carriers. Discover Chemical Engineering. 2022;2(1):1–50.
75. Larring Y, et al. Evaluation of a mixed Fe–Mn oxide system for chemical looping combustion. Energy Fuels. 2015;29(5):3438–45.
76. Zhou, Z., M.P. Harold, and D. Luss, *Dynamic Oxygen Storage Capacity of Ceria-Zirconia and Mn0. 5Fe2. 5O4 Spinel: Experiments and Modeling.* Industrial & Engineering Chemistry Research, 2021. **60**(18): p. 6465–6482.
77. De Vos Y, et al. Development of Stable oxygen carrier materials for chemical looping processes—A review. Catalysts. 2020;10(8):926.
78. Tian M, et al. Recent advances of oxygen carriers for chemical looping reforming of methane. ChemCatChem. 2021;13(7):1615–37.
79. Chen, P.W., et al., *CH 4 steam reforming on Pt+ Pd/Al 2 O 3 monolith: impact of Mn 0.5 Fe 2.5 O 4 spinel addition.* Catalysis Science & Technology, 2022. **12**(8): p. 2618–2633.
80. Zeng D, et al. Ternary mixed spinel oxides as oxygen carriers for chemical looping hydrogen production operating at 550° C. ACS Appl Mater Interfaces. 2019;11(47):44223–32.
81. Wei G, et al. Reaction performance of Ce-enhanced hematite oxygen carrier in chemical looping reforming of biomass pyrolyzed gas coupled with CO2 splitting. Energy. 2021;215: 119044.
82. Lee, K. and J.R. Scheffe, *Characterization of a laser-based heating system coupled with in operando Raman spectroscopy for studying solar thermochemical redox cycles.* Journal of Solar Energy Engineering, 2019. **141**(2).
83. Sediva E, et al. Evaluating the Redox Behavior of Doped Ceria for Thermochemical CO2 Splitting Using Time-Resolved Raman Spectroscopy. ACS Applied Energy Materials. 2021;4(2):1474–83.
84. Feng K, et al. In-situ/operando techniques to identify active sites for thermochemical conversion of CO2 over heterogeneous catalysts. J Energy Chem. 2021;62:153–71.
85. Morgan K, et al. Forty years of temporal analysis of products. Catal Sci Technol. 2017;7(12):2416–39.
86. Fushimi R, Gleaves J. Recent advances in dynamic chemical characterization using Temporal Analysis of Products. Curr Opin Chem Eng. 2018;21:10–21.
87. Gleaves JT, et al. Ethylene oxidation on silver powder: a TAP reactor study. J Catal. 1990;121(1):202–18.
88. Wang Y, et al. Rate/concentration kinetic petals: a transient method to examine the interplay of surface reaction processes. J Phys Chem A. 2019;123(40):8717–25.
89. Shekhtman SO, et al. "State defining" experiment in chemical kinetics—primary characterization of catalyst activity in a TAP experiment. Chem Eng Sci. 2003;58(21):4843–59.
90. Wenzel M, Rihko-Struckmann L, Sundmacher K. Continuous production of CO from CO2 by RWGS chemical looping in fixed and fluidized bed reactors. Chem Eng J. 2018;336:278–96.
91. Han, L., Z. Zhou, and G.M. Bollas, *Heterogeneous modeling of chemical-looping combustion. Part 1: Reactor model.* Chemical Engineering Science, 2013. **104**: p. 233–249.

92. Han, L., Z. Zhou, and G.M. Bollas, *Heterogeneous modeling of chemical-looping combustion. Part 2: Particle model.* Chemical Engineering Science, 2014. **113**: p. 116–128.
93. Metcalfe IS, et al. Overcoming chemical equilibrium limitations using a thermodynamically reversible chemical reactor. Nat Chem. 2019;11(7):638–43.
94. Bulfin B, Miranda M, Steinfeld A. Performance indicators for benchmarking solar thermochemical fuel processes and reactors. Frontiers in Energy Research. 2021;9: 677980.
95. Bulfin B, et al. Intensification of the reverse water–gas shift process using a countercurrent chemical looping regenerative reactor. Chem Eng J. 2023;461: 141896.